NANO LETTERS
Letter
Cite This: Nano Lett. 2018, 18, 7207−7210
pubs.acs.org/NanoLett

Active Two-Dimensional Steering of Radiation from a Nanoaperture

Laura S. Dreissen,[†] Hugo F. Schouten,[†] Wim Ubachs,[†,‡] Shreyas B. Raghunathan,[§] and Taco D. Visser*[,†,∥]

[†]Department of Physics and Astronomy, LaserLaB, Vrije Universiteit, De Boelelaan 1081, 1081 HV Amsterdam, The Netherlands
[‡]Advanced Research Center for Nanolithography, Science Park 110, 1098 XG Amsterdam, The Netherlands
[§]ASML, De Run 6501, 5504 DR Veldhoven, The Netherlands
[∥]Department of Physics and Astronomy, University of Rochester, Rochester, New York 14627, United States

ABSTRACT: We experimentally demonstrate control over the direction of radiation of a beam that passes through a square nanoaperture in a metal film. The ratio of the aperture size and the wavelength is such that only three guided modes, each with different spatial symmetries, can be excited. Using a spatial light modulator, the superposition of the three modes can be altered, thus allowing for a controlled variation of the radiation pattern that emanates from the nanoaperture. Robust and stable steering of 9.5° in two orthogonal directions was achieved.

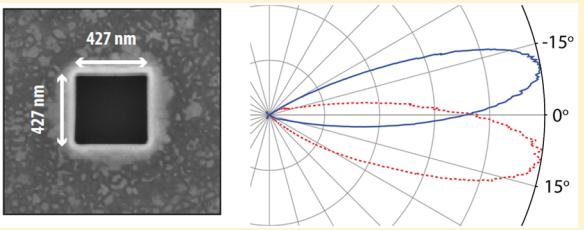

KEYWORDS: *Nanoapertures, radiation steering, diffraction, guided modes, optical switch*

Since the seminal work by Bethe,[1] many studies have been devoted to understanding the physical mechanisms that underly the transmission of radiation through nanoapertures,[2−11] a topic of both fundamental and technical interest. Several methods have been proposed to dynamically control the total transmission, in order to achieve all-optical switching.[12−14] A useful next step would be to actively steer the radiation, something of great importance for applications such as selective probing of nanosamples, and all-optical circuits for telecommunication. Directional transmission has been achieved, for example, by using a single subwavelength slit surrounded by surface corrugations or grooves,[15,16] and by varying the refractive index of neighboring subwavelength slits.[17] However, all these approaches lead to a static asymmetry of the radiated field. What has not been achieved so far is the possibility to dynamically steer the transmitted field in two orthogonal directions.

Here we report an experiment in which such steering is clearly demonstrated. Central to our approach is the selective excitation of guided modes in a wavelength-sized aperture in a metal film. We previously used a similar technique to control the direction in which surface plasmon polaritons are launched,[18] and to obtain one-dimensional beam steering from a narrow slit.[19] A nontrivial extension to two-dimensional steering has now been realized by using a square aperture illuminated by light with a wavelength such that only three guided modes can be excited. Using a spatial light modulator the phase of each of the three modes is controlled. The transmitted field, which is a coherent superposition of these modes, can thus be altered, leading to a change in the directionality of the emanating field.

The radiation from an aperture can be understood by analyzing the guided (i.e., nonevanescent) modes that it can sustain. Consider a square hole with sides a in a perfect conductor such that

$$\lambda < a < \frac{\sqrt{5}}{2}\lambda \tag{1}$$

where λ denotes the free-space wavelength. If the incident field of frequency ω is x-polarized, only three modes can be excited,[20] namely TE_{01}, TE_{02}, and a hybrid TE_{11}/TM_{11} mode, the latter being such that $E_y = 0$. The x-component of the electric field of the mn-mode is given by the expression

$$E_{x;mn}(\mathbf{r}, t) = A_{mn} \cos\left(\frac{m\pi x}{a}\right)\sin\left(\frac{n\pi y}{a}\right)\exp[\mathrm{i}(k_z z - \omega t)] \tag{2}$$

where $\mathbf{r} = (x,y,z)$ is a point in space, t is a moment in time, A_{mn} is an amplitude, and k_z denotes the effective longitudinal wavenumber of the mode. In eq 2, the origin of the coordinates is taken at the bottom left corner of the aperture. The spatial symmetry properties of each mode with respect to the center of the aperture are listed in Table 1. It is seen that every mode displays a unique combination of symmetries in the x- and y-direction. As will be shown shortly, by considering modes with

Table 1. Symmetries of E_x of Guided Modes

mode	x-direction	y-direction
TE_{01}	even	even
TE_{02}	even	odd
TE_{11}/TM_{11}	odd	even

Received: August 15, 2018
Revised: October 5, 2018
Published: October 29, 2018

DOI: 10.1021/acs.nanolett.8b03319
Nano Lett. 2018, 18, 7207−7210

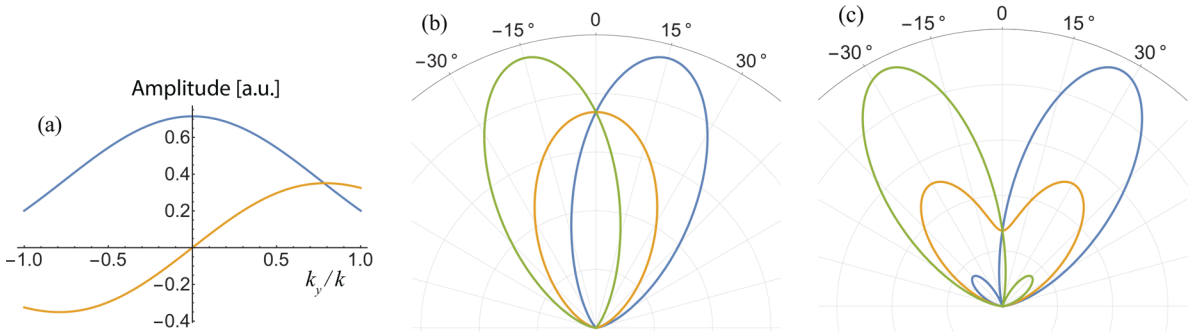

Figure 1. Principle of radiation steering. (a) The far zone field amplitude along the y-direction due to the TE_{01} mode (blue) and the TE_{02} mode (orange). (b) Polar plot of the radiated intensity for three values of the relative phase: $\delta_2 = 0$ (blue), $\delta_2 = \pi/2$ (orange), and $\delta_2 = \pi$ (green). (a,b) The amplitude ratio is set to 0.6. (c) The ratio is increased to 2.0.

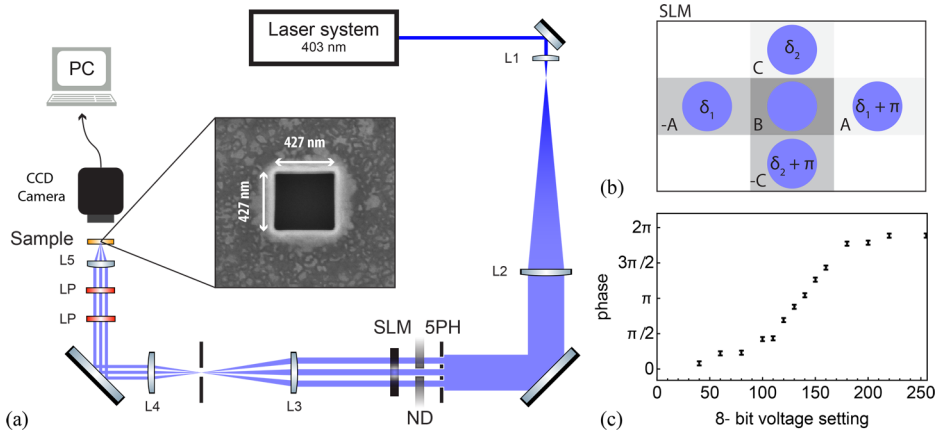

Figure 2. Schematic of the setup (a) with an electron microscope image of the gold sample (inset). The optical elements indicated with L1−L5 are lenses, LP are linear polarizers, ND are neutral density filters, and 5PH refers to a plate with five holes (see text). (b) Layout of the opaque plate with five holes. The fields passing through these holes are labeled A, −A, B, C, and −C, respectively. (c) Calibration curve of the phase change imparted by the SLM as a function of the applied gray level/voltage setting.

specific spatial symmetries in two dimensions, rather than one (as in 18 and 19), we can achieve active radiation steering in both the x- and y-direction.

For our method it is essential that the aperture is square-shaped with sides given by eq 1. Only then does a degenerate, hybrid TE_{11}/TM_{11} mode exist, and only then does the aperture allow exactly three guided modes with the right spatial symmetries. It is unclear if the same goal of selective excitation of nonevanescent modes with a prescribed symmetry could be achieved with a circular aperture.

The radiated electric field due to each mode can be calculated using the far-field diffraction formula[20]

$$\mathbf{E}_{mn}(\mathbf{r}) = \frac{ie^{ikr}}{2\pi r}\mathbf{k} \times \int_{-a/2}^{a/2}\int_{-a/2}^{a/2} \mathbf{n} \times \mathbf{E}_{mn}(\mathbf{r}')e^{-i\mathbf{k}\cdot\mathbf{r}'}dx'\,dy' \tag{3}$$

$$= A_{mn}\frac{ie^{ikr}}{2\pi r}\mathbf{k} \times (0, \tilde{E}_{mn}, 0)^T \tag{4}$$

where

$$\tilde{E}_{mn}(k_x, k_y) = \int_{-a/2}^{a/2}\int_{-a/2}^{a/2} \cos\left[\frac{m\pi(x' + a/2)}{a}\right]\sin\left[\frac{n\pi(y' + a/2)}{a}\right] e^{-i(k_x x' + k_y y')}dx'\,dy' \tag{5}$$

k is the free-space wavenumber, $\mathbf{k} = k\mathbf{r}/|\mathbf{r}|$, $\mathbf{n} = (0,0,1)$, and T denotes the transpose. Also, a change of variables was applied to shift the origin of the coordinate system to the center of the aperture, and the time dependence has been suppressed for brevity. Carrying out the integration in eq 5 gives, apart from constant phase factors, that

$$\tilde{E}_{01}(k_x, k_y) = \frac{2\sin\left(\frac{k_x a}{2}\right)}{k_x}\frac{2\pi a}{\pi^2 - a^2k_y^2}\cos\left(\frac{k_y a}{2}\right) \tag{6}$$

$$\tilde{E}_{02}(k_x, k_y) = \frac{2\sin\left(\frac{k_x a}{2}\right)}{k_x}\frac{4\pi a}{4\pi^2 - a^2k_y^2}\sin\left(\frac{k_y a}{2}\right) \tag{7}$$

$$\tilde{E}_{11}(k_x, k_y) = \frac{2k_x a^2}{\pi^2 - a^2k_x^2}\cos\left(\frac{k_x a}{2}\right)\frac{2\pi a}{\pi^2 - a^2k_y^2}\cos\left(\frac{k_y a}{2}\right) \tag{8}$$

The radiated intensity $I = \mathbf{S}\cdot\mathbf{r}$ with $\mathbf{S}$ the Poynting vector, is given by the sum of the three modal contributions, that is

$$I(k_x, k_y) \propto (k^2 - k_y^2)|A_{01}\tilde{E}_{01} + A_{11}e^{i\delta_1}\tilde{E}_{11} + A_{02}e^{i\delta_2}\tilde{E}_{02}|^2 \tag{9}$$

where δ_1 and δ_2 indicate the phase of the TE_{11}/TM_{11} and TE_{02} modes with respect to the TE_{01} mode at the exit plane of the aperture. By changing the phase δ_1 we can steer the radiated intensity along the x direction, whereas changing δ_2 steers the radiation in the y-direction. This principle is illustrated in Figure 1 for the case of just two modes. The left-hand panel

DOI: 10.1021/acs.nanolett.8b03319
Nano Lett. 2018, 18, 7207−7210

(a) shows the individual far-zone fields, $\tilde{E}_{01}$ and $\tilde{E}_{02}$, that are due to the TE_{01} and the TE_{02} mode, respectively. In panel (b), the radiated intensity generated by the superposed modes is plotted for three values of their relative phase δ_2. The maximum steering angle can be increased by increasing the amplitude ratio. An example is shown in panel (c), However, as can be seen, this leads to a broader radiation pattern for $\delta_2 = \pi/2$ and to side lobes for the other values of δ_2.

A sketch of the experimental setup is shown in Figure 2a. A continuous-wave laser was used, operating at 403 nm, with a bandwidth of 2 MHz, and an output power of ~300 mW of which only a small fraction was used.[21] After expansion and beam cleaning the homogeneous, flat wavefront is passed through an opaque plate with five identical circular holes, each with a 2 mm diameter and a center-to-center distance of 4 mm (panel b). The plate is put directly in front of a spatial light modulator (SLM) that works in transmission (Holoey LC 2012). The SLM is used to imprint a specific phase onto each of the five transmitted beams. The induced phase change as a function of the applied gray level (i.e., voltage setting) was determined by observing the transverse shift in a two-slit interference pattern. The resulting calibration curve is plotted in panel c.

The inset of panel a shows the sample. It consists of a square aperture (427 × 427 nm), etched by a focused ion beam in a 350 nm thick gold film that is mounted on a glass substrate. The aperture size is such that eq 1 is satisfied for a wavelength of 403 nm. The film thickness ensures that the intensity of the field that is directly transmitted through the sample is negligable.

From panel b of Figure 2 it is seen that field B passes through the central hole of the opaque plate that covers the SLM. This field is normally incident onto the aperture, and thus has an even symmetry in both the x and y direction. According to Table 1, this means that field B only excites the TE_{01} mode. The fields C and −C, which pass through the top and bottom holes, get an imprinted phase of δ_2 and $\delta_2 + \pi$, respectively. The combination of these two fields with opposite phase is therefore antisymmetric in the y-direction and symmetric in the x-direction. Hence this combined field will only excite the TE_{02} mode. The phase of the fields A and −A, which travel through the left and right hole, is set to δ_1 and $\delta_1 + \pi$, respectively. Because the combination of these two fields is antisymmetric in the x direction and symmetric in the y-direction, this will excite just the hybrid TE_{11}/TM_{11} mode. By changing δ_1 and δ_2 the relative phase of each of the three guided modes that are excited in the aperture can be controlled. Neutral density filters are placed in front of each outer hole to modulate the intensity of the corresponding beams. A combination of two linear polarizers, before lens 5, is used to modulate the intensity of the central beam and ensure x-polarized light. Together this gives us complete control over the superposition of the guided modes, that is, the total field in the aperture.

Our experimental results clearly demonstrate the abilty to steer the radiation. Four measured radiation patterns, which are maximally steered in either the x or the y direction, are shown in Figure 3. A deflection of ±9.5° in both directions was achieved. Simultaneous variation of the phases δ_1 and δ_2 allows us to shift the radiation two dimensionally in a continuous fashion. The setup, built from standard mirror mounts, proved to be very stable with the radiation pattern undergoing no significant change over a period of hours. This is a significant

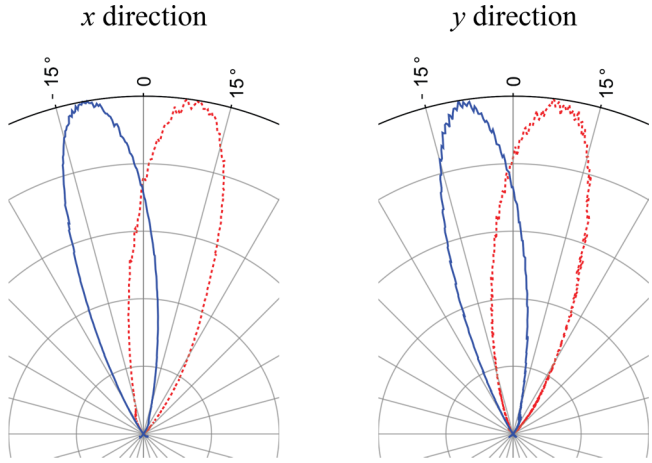

Figure 3. Polar plot of the measured radiation pattern for maximum steering in the x- and y-direction. Zero degrees indicates the forward direction, normal to the metal film. Blue curves: $\delta_1 = 0$ and $\delta_2 = 0$. Red curves: $\delta_1 = \pi$ and $\delta_2 = \pi$.

improvement of the stability obtained in 19. The efficiency of the setup, that is, the ratio of the power that is transmitted by the aperture and the power of the focused field, is largely determined by the Fresnel number of L5, the last lens.

Simulated and observed intensities captured with a charge-coupled device (CCD) camera are shown in Figure 4. The left-hand column shows the measured intensity patterns for maximum steering angles −9.5° and 9.5° in two orthogonal directions. The right-hand column shows a simulation, based on eq 9, for four different setings of δ_1 and δ_2. The amplitudes were chosen to obtain a reasonable qualitative agreement between the simulations and the measurements. A less than perfect agreement is to be expected, because the simulated results are for the idealized case of a perfectly conducting metal film. This assumption leads to narrower modes and hence a broader radiation pattern. Also, the precise value of the mode amplitudes is not known. Furthermore, the uncertainty in the angles of observation is approximately 1°.

We note that for the particular SLM that was available, a change in the phase setting also produced a change in the amplitude and state of polarization. Therefore, variable neutral density filters were used to ensure that the mode amplitudes remained approximately equal after δ_1 and δ_2 had been varied. The use of a more advanced SLM device[22,23] would make this amplitude adjustment and correction for polarization changes unnecessary.

In our earlier work,[19] we obtained one-dimensional steering from a nanoslit. The current setup is much simpler, involves only one optical path and is significantly more stable. A piezo element is no longer required, and the use of a thicker film has solved the issue of direct transmission leaking through the sample. And, of course, dynamic two-dimensional steering is now obtained.

We emphasize that our experiment provides a proof of principle of active, two-dimensional beam steering. The effect that we observe is a linear optical phenomenon, meaning that a high power laser, as was used in our setup, is not necessary. The phenomenon of beam steering is scalable to the low power levels that may be produced and handled "on-chip" in semiconductor devices. In our experiment, a laser with a very long coherence length (2 MHz optical bandwidth) was used. However, because our setup essentially uses a single optical

DOI: 10.1021/acs.nanolett.8b03319
Nano Lett. 2018, 18, 7207−7210

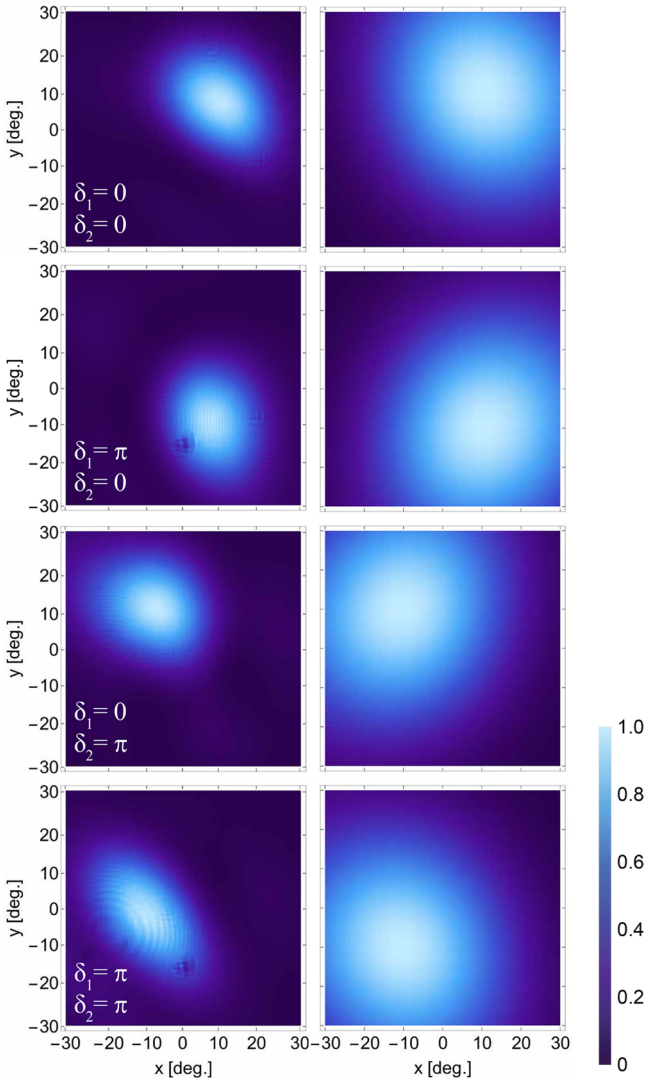

Figure 4. Observed CCD images (left column) and simulated images (right column) of two-dimensional beam steering. In the simulations A_{11} = 0.6 and A_{02} = 0.4.

path, a shorter coherence length would also suffice. The 403 nm wavelength was chosen to obtain the full 2π phase range of the specific SLM that was used. Our technique can be applied at different wavelengths, provided that the inequalities (1) that relate the aperture size a to the wavelength λ, are satisfied and the SLM provides a full 2π phase range. For example, for the choice of a telecom wavelength λ = 1500 nm, the required value of the aperture size would be 1500 nm $\leq a \leq$ 1677 nm. It is worth noting that the maximum steering angle can be tuned by changing the relative amplitudes of the modes, although larger steering angles are accompanied by a broadening of the radiation pattern and the onset of side lobes as was shown in Figure 1.

In conclusion, we have demonstrated dynamic control of the direction of radiation that emanates from a narrow square aperture in a metal film. This was accomplished by selective excitation of the three guided modes that such an aperture allows. Our method uses only an SLM and does not involve any mechanical adjustment of optical elements. A simple wave-guiding model provides physical understanding and, even though it assumes perfect conductivity, gives good qualitative agreement with the experimental results. Unlike previously reported static configurations,[15−17] our dynamic setup can be used as an optical switch in photonic circuitry in which light is sent to different ports, or in optical biosensors in which samples need to be scanned.

AUTHOR INFORMATION

Corresponding Author

*E-mail: t.d.visser@vu.nl.

ORCID

Taco D. Visser: 0000-0002-6269-1068

Notes

The authors declare no competing financial interest.

ACKNOWLEDGMENTS

The authors wish to thank Andries Lof of AMOLF NanoCenter Amsterdam for fabrication of the sample. T.D.V. acknowledges support from the Air Force Office of Scientific Research under award number FA9550-16-1-0119.

REFERENCES

(1) Bethe, H. A. *Phys. Rev.* **1944**, *66*, 163−182.
(2) Bouwkamp, C. J. *Rep. Prog. Phys.* **1954**, *17*, 35−100.
(3) Ebbesen, T. W.; Lezec, H. J.; Ghaemi, H. F.; Thio, T.; Wolff, P. A. *Nature* **1998**, *391*, 667−669.
(4) Ghaemi, H. F.; Thio, T.; Grupp, D. E.; Ebbesen, T. W.; Lezec, H. J. *Phys. Rev. B: Condens. Matter Mater. Phys.* **1998**, *58*, 6779−6782.
(5) Schouten, H. F.; Visser, T. D.; Gbur, G.; Lenstra, D.; Blok, H. *Opt. Express* **2003**, *11*, 371−380.
(6) Schouten, H. F.; Visser, T. D.; Gbur, G.; Lenstra, D.; et al. *Phys. Rev. Lett.* **2004**, *93*, 173901.
(7) Degiron, A.; Lezec, H. J.; Yamamoto, N.; Ebbesen, T. W. *Opt. Commun.* **2004**, *239*, 61−66.
(8) García-Vidal, F. J.; Moreno, E.; Porto, J. A.; Martín-Moreno, L. *Phys. Rev. Lett.* **2005**, *95*, 103901.
(9) Liu, H.; Lalanne, P. *Nature* **2008**, *452*, 728−731.
(10) García-Vidal, F. J.; Martín-Moreno, L.; Ebbesen, T. W.; Kuipers, L. *Rev. Mod. Phys.* **2010**, *82*, 729−787.
(11) Genet, C.; Ebbesen, T. W. *Nature* **2007**, *445*, 39−46.
(12) Kim, T. J.; Thio, T.; Ebbesen, T. W.; Grupp, D. E.; Lezec, H. J. *Opt. Lett.* **1999**, *24*, 256−258.
(13) Pacifici, D.; Lezec, H. J.; Atwater, H. A. *Nat. Photonics* **2007**, *1*, 402−406.
(14) Daniel, S.; Saastamoinen, K.; Saastamoinen, T.; Rahomaki, J.; Friberg, A. T.; Visser, T. D. *Opt. Express* **2015**, *23*, 22512−22519.
(15) García-Vidal, F. J.; Martín-Moreno, L.; Lezec, H. J.; Ebbesen, T. W. *Appl. Phys. Lett.* **2003**, *83*, 4500−4502.
(16) Wang, C.; Du, C.; Luo, X. *Phys. Rev. B: Condens. Matter Mater. Phys.* **2006**, *74*, 245403.
(17) Vincenti, M. A.; D'Orazio, A.; Buncick, M.; Akozbek, N.; Bloemer, M. J.; Scalora, M. *J. Opt. Soc. Am. B* **2009**, *26*, 301−307.
(18) Raghunathan, S. B.; Gan, C. H.; van Dijk, T.; Ea Kim, B.; Schouten, H. F.; Ubachs, W.; Lalanne, P.; Visser, T. D. *Opt. Express* **2012**, *20*, 15326−15335.
(19) Raghunathan, S. B.; Schouten, H. F.; Ubachs, W.; Kim, B.; Gan, C. H.; Visser, T. D. *Phys. Rev. Lett.* **2013**, *111*, 153901.
(20) Jackson, J. D.; *Classical Electrodynamics*, 3rd ed.: Wiley: New York, 1999; Section 8.4 and Chapter 10.
(21) Gu, Z.; Vieitez, M. O.; van Duijn, E. J.; Ubachs, W. *Rev. Sci. Instrum.* **2012**, *83*, 053112.
(22) Chen, H.; Hao, J.; Zhang, B.; Xu, J.; Ding, J.; Wang, H. *Opt. Lett.* **2011**, *36*, 3179−3181.
(23) Moreno, I.; Davis, J. A.; Hernandez, T. M.; Cottrell, D. M.; Sand, D. *Opt. Express* **2012**, *20*, 364−376.

DOI: 10.1021/acs.nanolett.8b03319
Nano Lett. 2018, 18, 7207−7210